

## Pressure-induced Hall-effect spectroscopy of silicon $DX$ states in planar doped GaAs-AlAs superlattices

P. Sellitto, J. Sicart,\* and J. L. Robert

*Groupe d'Etude des Semiconducteurs, Université Montpellier II, F 34095 Montpellier Cédex 05, France*

R. Planel

*Laboratoire Microstructures et Microélectronique, F 92220 Bagneux, France*

(Received 14 June 1994; revised manuscript received 18 November 1994)

To determine the energetical separation between the silicon  $DX$  states in  $\text{Al}_x\text{Ga}_{1-x}\text{As}$  compounds, we used planar doped GaAs-AlAs superlattices and we tuned the conduction miniband energy by applying hydrostatic pressure. When pressure is applied, the miniband energy crosses over the deep levels while shallow levels are linked to the miniband. Hall measurements performed on selectively doped superlattices allow us to derive the ionization energies of the silicon donor in the framework of the  $DX$ -donor model with negative correlation energy. We found four deep states energetically separated one from the other by about 40 meV.

### I. INTRODUCTION

Silicon is a dopant impurity which gives both shallow and deep levels in GaAs, AlAs, and  $\text{Al}_x\text{Ga}_{1-x}\text{As}$ . Shallow levels are described in terms of the effective-mass theory whereas deep states are related to relaxed donors according to the atomic environment of the silicon site. The deep donor levels (so-called  $DX$  states) have been observed in many III-V semiconductors.<sup>1,2</sup> In  $\text{Al}_x\text{Ga}_{1-x}\text{As}$ , for example, they control the electrical conductivity of the material when  $x > 0.22$  and are responsible for peculiar properties such as persistent photoconductivity, large photoionization energy, and large pressure-induced carrier freeze-out. Therefore they have been extensively studied in the last ten years. Despite the fact that the microscopic structure of the deep donor remains controversial, the description of the metastable  $DX$  center in terms of relaxation of the crystal lattice and negative charge of the ground state  $DX^-$  is widely admitted.<sup>3</sup> These characteristics are supported by a lot of electrical and optical measurements such as Hall, photo-Hall, capacitance, and transient spectroscopy experiments.<sup>4-8</sup>

In addition, hydrostatic pressure which modifies the conduction-band structure in a way similar to increasing the alloy composition<sup>9</sup> (i.e., the Al fraction) has been used to study the relationship of the deep level to the band structure. In particular, the discrete structure of the  $DX$  center has been demonstrated in many experiments,<sup>10-12</sup> and in  $\text{Al}_x\text{Ga}_{1-x}\text{As}$  doped with silicon four levels have been assigned to the Al environment of the silicon atom. They have been denoted as  $DX_i$ , where the index takes the values 0, 1, 2, and 3 corresponding, respectively, to the number of Al near-neighbor atoms. However, the effects of the  $DX$  center splitting on the properties of complex heterostructures, including superlattices and quantum wells have not yet been extensively investigated.<sup>13-15</sup>

The aim of this paper is to study the behavior of the

silicon impurity in GaAs-AlAs short-period superlattices. The main advantage in using superlattices instead of a semiconducting alloy lies in the fact that first, Ga and Al atoms are separated spatially while alloying effect stays only at the interfaces, second the conduction band can be tuned by varying the period of the superlattice.<sup>16</sup> Consequently, the study of the  $DX_i$  states is easier since doping the superlattice selectively in the GaAs or AlAs layers, or at the interfaces, allows us to isolate each  $DX$  state, which is impossible to achieve in the alloy. Moreover, the possibility to tune the superlattice conduction miniband energy allows us to fix it below (above) the  $DX_i$  state, making it a resonant (nonresonant) state. These two approaches to  $DX$  center characterization in short-period superlattices need to be combined in order to isolate each  $DX$  level, but the ideal structure is controlled by a technological limitation, i.e., the dopant interdiffusion.<sup>17</sup> This is the reason we used planar-doped (so called  $\delta$ -doped) short-period superlattices in this work.

By applying hydrostatic pressures up to 12 kbar, we induced a positive shift of the conduction miniband energy. Consequently, the miniband edge crossed over the resonant  $DX_i$  state making it a nonresonant state in the gap of the superlattice. When several  $DX$  states are present in the superlattice, this method allows us to achieve an energetical spectroscopy of the levels, and the ionization energy is derived from the analysis of the Hall data under pressure.

The paper is organized as follows. Results of Hall and photo-Hall measurements performed on uniformly and  $\delta$ -doped superlattices are given, focusing on the activation energy of the silicon donor and persistent photoconductivity effects. Then Hall measurements performed under hydrostatic pressure are reported, and the method for achieving a spectroscopy of the donor levels is described. Finally, the formalization in fitting experimental data is given and applied on samples to calculate the ionization energy  $E_{DX_i}$  of the silicon deep donor.

TABLE I. Hall and photo-Hall data at room temperature (RT) and at 77 K (LN). The activation energy  $E_{\text{act}}$  corresponds to the activation energy of the carrier concentration at high temperatures.  $N_{\text{Si}}$  denotes the nominal sheet silicon concentration introduced during the planar doping step ( $3.3 \times 10^{20} \text{ m}^{-2}$ ) and averaged on the whole sample thickness in order to be compared to electrical data. Samples  $\partial$ -doped at the interface differed by the silicon incorporation sequence, i.e., the doping plane was deposited on the GaAs layer in samples HC07 and on the AlAs layer in sample HC03, respectively.  $N_{\text{pc}}$  denotes the Hall carrier concentration measured at 77 K under LED illumination.

| Sample                 |                          | HB11             | HC01             | HB01    | HC03                  | HC07                  |
|------------------------|--------------------------|------------------|------------------|---------|-----------------------|-----------------------|
| Doped in               | Units                    | $\partial$ -GaAs | $\partial$ -AlAs | Uniform | $\partial$ -Interface | $\partial$ -Interface |
| $N_{\text{Si}}$        | $10^{22} \text{ m}^{-3}$ | 9                | 9                | 6       | 9                     | 9                     |
| $N$ (RT)               | $10^{22} \text{ m}^{-3}$ | 7.3              | 6                | 4.2     | 4.8                   | 5.8                   |
| $\mu$ (RT)             | $\text{cm}^2/\text{Vs}$  | 1885             | 1800             | 2100    | 1656                  | 1295                  |
| $N$ (LN)               | $10^{22} \text{ m}^{-3}$ | 5.6              | 1                | 2.5     | 2.5                   | 1.7                   |
| $\mu$ (LN)             | $\text{cm}^2/\text{Vs}$  | 2260             | 1780             | 2230    | 1942                  | 1460                  |
| $N_{\text{pc}}$ (LN)   | $10^{22} \text{ m}^{-3}$ | 7.3              | 7.2              | 4.5     | 5.3                   | 6.4                   |
| $\mu_{\text{pc}}$ (LN) | $\text{cm}^2/\text{Vs}$  | 2314             | 2400             | 2320    | 2167                  | 1753                  |
| $E_{\text{act}}$       | meV                      | 5                | 45               | 11      | 14                    | 27                    |

## II. MATERIALS AND METHODS

The samples were grown by molecular-beam epitaxy at 550°C. They were formed from 135 periods of GaAs-AlAs deposited on a 500-nm-thick layer of  $\text{Al}_{0.33}\text{Ga}_{0.67}\text{As}$  and separated from the substrate by an undoped GaAs buffer layer. A 10-nm-thick layer of GaAs was deposited as capping layer. The nominal period of the superlattice was 37 Å and the equivalent Al content was  $x = 0.23$  (i.e., GaAs well width  $W_G = 28.5$  Å and AlAs barrier width  $W_A = 8.5$  Å respectively). The growth was halted during the silicon introduction (planar doping technique). The nominal silicon sheet density was  $3.3 \times 10^{10} \text{ cm}^{-2}$  per plane, yielding a maximum of silicon concentration of  $9 \times 10^{16} \text{ cm}^{-3}$  averaged on the whole superlattice thickness. Sample HB01 was doped uniformly at  $6 \times 10^{16} \text{ cm}^{-3}$  both in GaAs and AlAs layers for comparison. Samples  $\partial$ -doped at the interface differed by the silicon incorporation sequence, i.e., the doping plane was deposited on the GaAs layer in samples HC07 and on the AlAs layer in sample HC03 respectively. Table I gives Hall and photo-Hall data at room temperature and 77 K,

respectively. Figures 1 and 2 show the Arrhenius plots of the Hall-carrier concentration and Hall mobility, respectively. Photo-Hall measurements achieved under light-emitting diode (LED) illumination show that both carrier concentration and mobility increased as observed in the silicon doped  $\text{Al}_x\text{Ga}_{1-x}\text{As}$  alloy.<sup>18</sup> The carrier concentration did not change when the LED was switched off at 77 K, leading to the well-known persistent photoconductivity effect (PPC). Note that the PPC increase was very low in samples  $\partial$ -doped in the GaAs layers. When temperature was raised, the photo-Hall concentration increased whereas the carrier concentration recovered its value in the dark due to the slow capture of electrons from the conduction band onto the  $DX$  levels. The photo-Hall carrier concentration shows a maximum corresponding to a value close to the total electrical activity  $N_d - N_a$  assuming complete ionization of silicon. Indeed, photoionization under LED exposure would lead to a total excitation of electrons from all silicon donor levels into the conduction miniband. When comparing this value to that of the nominal silicon concentration, the corresponding compensating concentration  $N_a$  can be estimated ranging between  $1 \times 10^{16}$  and  $1.8 \times 10^{16} \text{ cm}^{-3}$  depending on the sample. The Arrhenius plot Fig. 1 exhib-

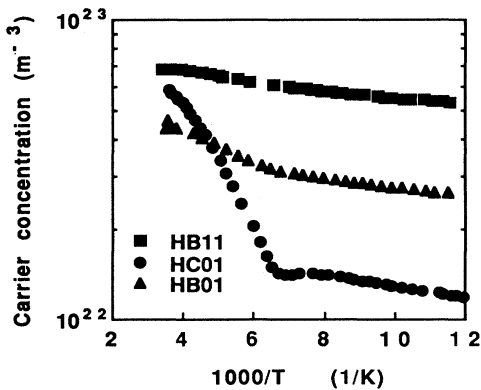


FIG. 1. Arrhenius plot of the Hall-carrier concentration in samples doped uniformly (HB01) and selectively in GaAs (HB11) or AlAs (HC01), respectively.

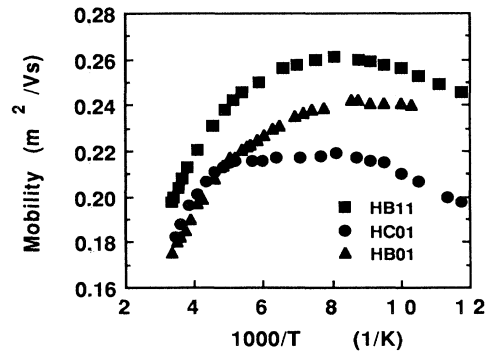


FIG. 2. Hall mobility vs  $1000/T$  for the same samples as in Fig. 1.

ited two slopes corresponding to the thermal activation of the deep donor at high temperatures and of the shallow donor at low temperatures. Values of the activation energy are collected in Table I, and they depended on the location of the dopant. The activation energy was larger when the dopant is introduced in the AlAs layers than in the GaAs layers, respectively. An intermediate value was measured in the uniformly doped sample or when doping at the interface. This experimental fact indicates clearly that the measured activation energy is associated with the  $DX_i$  levels,  $DX_0$  being the highest state and  $DX_3$  the lowest state according to the relative energies found previously in the alloy.

The miniband formation was described in the framework of the Kronig-Penney picture. We calculated that the conduction miniband was a  $\Gamma$ -type miniband located at 175 meV above the  $\Gamma$  band of the GaAs well. The shallow donor level which is present in all samples and thermally activated (a few meV at low temperatures) is linked with the  $\Gamma$  miniband. This assumption will be confirmed in Sec. III by performing Hall measurements under hydrostatic pressure. Thus the  $DX$  levels are resonant states for  $E_{DX} > 175$  meV and nonresonant states (i.e., in the gap of the superlattice) for  $E_{DX} < 175$  meV. As demonstrated in a previous paper,<sup>17</sup> the outdiffusion of dopant atoms in the adjacent layers is a limitation in using selectively doped short-period superlattices. This interdiffusion is the result of a dopant segregation in the growing layer during its incorporation. It must be eliminated (or strongly reduced) in order to reduce the formation of additional  $DX$  levels at the interface or in adjacent layers. Indeed the existence of more than one  $DX$  levels at the interface or in adjacent layers complicates the interpretation of Hall data. For instance, we must assume the existence of two deep donors ( $DX_0$  and  $DX_3$ , respectively) in the uniformly doped superlattice.

Thus, to know if another  $DX$  level due to the outdiffusion of the dopant in the adjacent layer through the GaAs-AlAs interface was involved in interpreting Hall data in our  $\delta$ -doped samples, we performed thermal-

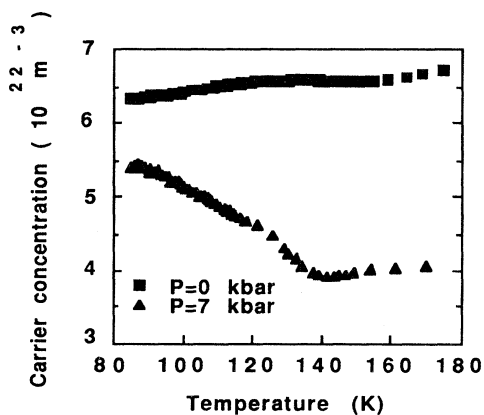


FIG. 3. Hall carrier concentration vs temperature in sample HB11  $\delta$ -doped in GaAs at two pressures. The sample was illuminated at low temperature during a short time and then heated at a constant rate (1 K/min).

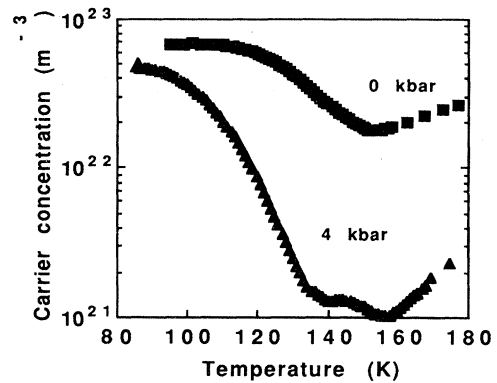


FIG. 4. Hall-carrier concentration vs temperature in sample HC01  $\delta$ -doped in AlAs at two pressures. The experiment procedure was the same as in Fig. 3.

ly stimulated capture/emission experiments (Figs. 3 and 4). Indeed it has been demonstrated that this technique reveals the multilevel structure of the  $DX$  center in the alloy.<sup>7,11</sup> The method consists of cooling the sample in darkness below the temperature of metastability of the  $DX$  level. Then the sample is illuminated yielding persistent photoconductivity (PPC), i.e., carriers are photoexcited from the  $DX$  into the conduction miniband. When the sample is heated with a constant sweep rate, carriers are captured from the miniband onto the  $DX$  levels. As demonstrated previously,<sup>15</sup> if several  $DX_i$  levels are involved in the thermal capture/emission mechanisms, the curves exhibit several steps. Indeed, at temperatures corresponding to the discrete distribution of the  $DX_i$  thermal emission energies, thermal capture is balanced for a short while by thermal emission of electrons from the  $DX$  level having the lowest emission energy into the conduction miniband. Consequently, this experiment gave an additional proof of the existence of several levels lying in the gap of the superlattice under pressure.

Finally, to interpret Hall data properly and to derive the energy of the  $DX$  states, we carried out electrical

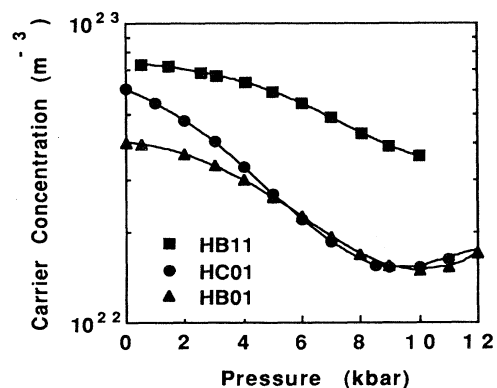


FIG. 5. Hall-carrier concentration vs pressure at room temperature in samples doped uniformly (HB01) and selectively in GaAs (HB11) or AlAs (HC01), respectively.

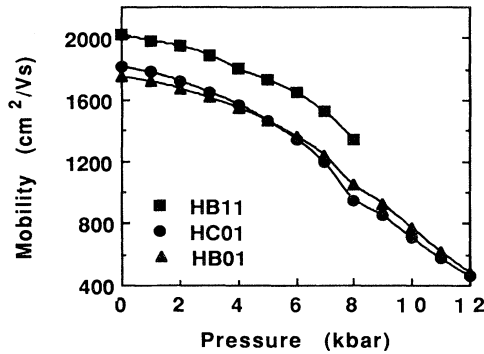


FIG. 6. Hall mobility vs pressure at room temperature in the same samples as in Fig. 5.

measurements under hydrostatic pressure (Figs. 5–8). The pressure was supplied by a gaz compressor Unipress apparatus (range 0–12 kbar). We also performed thermally stimulated electron emission experiments (Figs. 9 and 10) using the pressure-induced freeze-out (PIFO) technique.<sup>19</sup>

### III. HALL AND PHOTO-HALL DATA

As mentioned above, the interpretation of Hall data in semiconductors with several donor levels needs to be made carefully since the activation energy measured at high temperatures corresponds to an equivalent donor state. The largest ionization energy is measured in sample HC01  $\delta$ -doped in AlAs layers, confirming the existence of the low-lying  $DX_3$  level. However, the small energy (5 meV) measured in sample HB 11  $\delta$ -doped in GaAs layers cannot be assigned to the  $DX_0$  level since the energy shift ( $\Delta E \approx 40$  meV) is too small in comparison with values found previously in the  $Al_xGa_{1-x}As:Si$  alloy and ranging between 60 and 120 meV. The reason is that depending on the dopant location, the  $DX$  level is resonant or in the gap of the superlattice such that the measured activation energy corresponds to a shallow donor or a deep donor state. Thus the low value of the activation energy measured in sample HB 11 corresponds to a shallow level linked with the miniband minimum. This

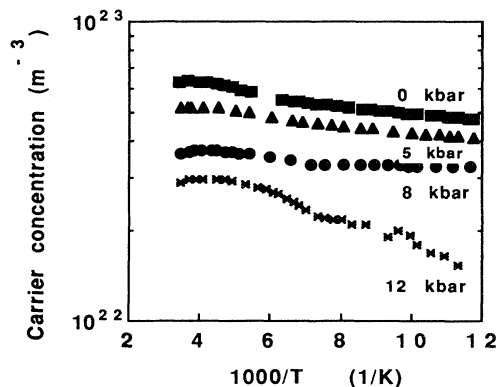


FIG. 7. Arrhenius plot of the Hall-carrier concentration in sample HB11 doped selectively in GaAs at various pressures.

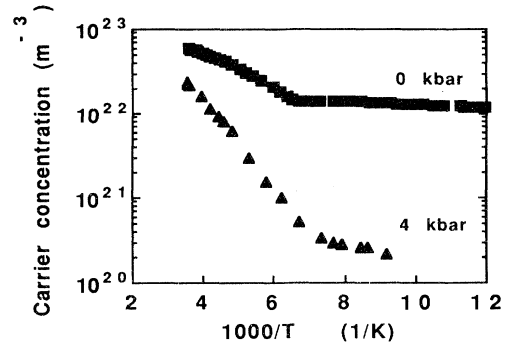


FIG. 8. Arrhenius plot of the Hall-carrier concentration in sample HC01 doped selectively in AlAs at various pressures.

interpretation will be confirmed by additional experiment performed under hydrostatic pressure and described in Sec. IV. When analyzing data in samples HC03 and HC07  $\delta$ -doped at the GaAs-AlAs interface, we find that sample HC03 shows an activation energy close to that of the uniformly doped sample (14 meV), whereas sample HC07 shows a larger energy (27 meV). This experimental fact denotes the outdiffusion of silicon atoms from the  $\delta$  plane in both adjacent layers. However, it is worth noting that since the difference between the two measured activation energies is large, this outdiffusion is rather due to a silicon segregation effect during the superlattice growth. The segregation length lies between 8 (the AlAs width) and 14 Å (half the GaAs width). Thus this kind of electrical experiment gives a better resolution than local probe techniques such as HRSIMS (high-resolution secondary-ion-mass spectrometry), HRXD (high-resolution x-ray diffraction), and LVM (local vibrational mode).<sup>20</sup> In order to prove this outdiffusion, we performed thermally stimulated electron-capture experiments in samples  $\delta$ -doped in GaAs and in samples  $\delta$ -doped in AlAs. Figures 3 and 4 show that these samples exhibit a two-step decrease of the Hall-carrier concentra-

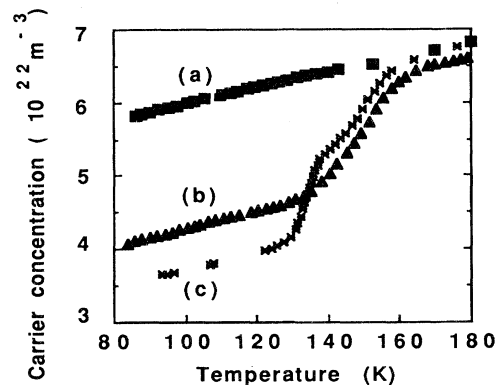


FIG. 9. Hall-carrier concentration vs temperature in sample HB11 doped selectively in GaAs. The PIFO procedure was applied on the sample, i.e., the sample was cooled under pressure (a)  $P=0$  kbar, (b)  $P=7$  kbar, and (c)  $P=12$  kbar, respectively. Then the pressure was released at 77 K and the temperature was increased with a constant heating rate (1 K/min).

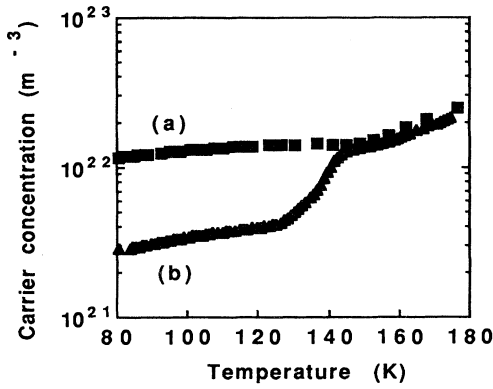


FIG. 10. Hall-carrier concentration vs temperature in sample HC01 doped selectively in AlAs. The experiment was achieved as in Fig. 9. (a) No applied pressure. (b) Sample cooled at 4 kbar.

tion under pressure, denoting the presence of an additional  $DX$  level in these samples.<sup>15</sup>

#### IV. HALL-EFFECT SPECTROSCOPY OF SILICON LEVELS UNDER HYDROSTATIC PRESSURE

In the following, we will use hydrostatic pressure to distinguish between hydrogeniclike shallow levels and deep localized  $DX_i$  states. Indeed it is well known that hydrogeniclike states are linked with their parent conduction-band minima while a strong shift of the localized levels is observed under pressure.<sup>19</sup> The metastable impurity (i.e., silicon  $DX$  center) leads to both deep and shallow levels coexisting in our superlattices. The shallow state is linked at few meV below the  $\Gamma$  miniband minimum, whereas the  $E_{DX_i}$  energy is assumed to be insensitive to the applied pressure.

By applying the pressure at room temperature, both Hall-carrier concentration and mobility decrease, as shown in Figs. 5 and 6, since the  $\Gamma$  miniband raises up by 10.8 meV/kbar and crosses at a pressure around 12 kbar over the  $X$  miniband moving down by 0.8 meV/kbar. Consequently, the  $DX$  states which are resonant states at zero pressure are empty at room temperature, and this decrease is interpreted as a mixed conduction (transition from a  $\Gamma$  conduction with high mobility to a  $X$  conduction with low mobility). In contrast, when a  $DX_i$  level becomes nonresonant by crossing down to the  $\Gamma$  miniband under pressure, a strong capture of electrons on the  $DX$  level arises leading to carrier freeze-out when pressure is released at low temperature (below the temperature of metastability of the deep level). In addition, the activation energy of the carrier concentration at high temperatures increased strongly when the deep state become lower than the shallow level at high pressures. Figures 7 and 8 show the Arrhenius plots at various pressures in samples HB11 and HC01, respectively. The existence of both shallow and  $DX_0$  states in GaAs is clearly demonstrated in sample HB11. Indeed, the activation energy did not change at pressures lower than 10 kbar, denoting

the existence of a shallow level linked with the miniband minimum. On the contrary, the activation energy increased at higher pressure, indicating the capture of electrons from the conduction miniband onto the deep  $DX$  level. The presence of more than one  $DX$  deep level is evidenced in samples HC01 and HB01, which behaved similarly. Indeed, since the  $DX_0$  state is the highest state and is involved only at pressures above 10 kbar in our superlattices, the behavior of both samples HB01 uniformly doped and HC01  $\delta$ -doped in AlAs at pressures lower than 10 kbar can be interpreted only by assuming the existence of two  $DX_i$  levels (a  $DX_3$  state in AlAs and an *interface* level). This result indicates that outdiffusion occurred in the sample  $\delta$ -doped in AlAs because of its small thickness (8 Å). We also performed electron thermal emission, carriers being freeze-out on the  $DX$  center after cooling the sample under pressure. The carrier concentration remained unchanged after releasing the pressure (PIFO technique<sup>19</sup>) and the sample was then heated with a constant heating rate (typically 1 K/min). The electron thermal emission depended on the involved deep  $DX$  level (Figs. 9 and 10). This experiment is an additional proof of the existence of a second  $DX$  donor level evidenced by the PIFO technique.

In order to make a quantitative analysis of Hall data given above and to derive the ionization energy of the different shallow and deep  $DX$  states, we have to develop the formalization of the Hall effect in superlattices with several states having positive and/or negative correlation energy.<sup>21</sup> It is assumed that both shallow and deep levels are related to the metastable silicon impurity in GaAs and AlAs. Thus the conservation of species and charges lead to Eqs. (1) and (2), respectively:

$$n = N_{d+} - N_{DX-} - N_a, \quad (1)$$

$$N_d = N_{d+} + N_{sd} + N_{DX^0} + N_{DX-}, \quad (2)$$

where  $N_{d+}$  is the total concentration of positively charged donors arising from the ionization of deep  $DX$  silicon states (double donors in density  $N_{DX-}$  with a negative correlation energy  $U$ ) as well as shallow silicon states (single donors in density  $N_{sd}$  with a positive correlation energy  $U$ ).  $N_d$  is the total donor concentration which cannot exceed the nominal silicon concentration assuming that each silicon atom acts as a donor atom. The concentration  $N_{DX^0}$  of the neutral state can be neglected in (1) because of the bistable character of the impurity:

$$2DX^0 \rightarrow d^+ + DX^-. \quad (3)$$

Assuming the  $U < 0$  character of the  $DX^-$  ground state, the total carrier concentration is given according to Theis, Mooney, and Parker<sup>22</sup>

$$n = N_d \frac{1 - \exp\left[-\frac{(E_f - E_{DX^-})}{kT}\right]}{1 + \exp\left[-\frac{E_f - E_{sd}}{kT}\right] + \exp\left[-\frac{(E_f - E_{DX^-})}{kT}\right]} - N_a, \quad (4)$$

where  $E_{sd}$  and  $E_{DX-}$  are the ionization energies of the shallow and deep states, respectively,  $N_a$  denoting the concentration of the compensating acceptor state. Equation (4) is the result of the application of the Fermi statistics on both single and double donor species of the multicharged  $DX$  state. The Hall-carrier concentration is fitted using a one-band model which takes into account the actual density of states in a superlattice with a  $\Gamma$  conduction miniband (see Ref. 17 for details). It is worth mentioning that the contribution of a  $X$  miniband conduction must be taken into account (mixed conduction formalism) when high pressure is applied on the samples, the  $\Gamma$ - $X$  crossover occurring at  $P = 12$  kbar in our superlattices.

The fit of the Arrhenius plot is made taking into account the dependance of the  $\Gamma$  and  $X$  minima with temperature (in K) and pressure (in kbar) as given in the literature:<sup>23</sup>

$$E_{\Gamma}(T,P) = 1.519 - [5.40 \times 10^{-4} T^2 / (T + 204)] + 0.0115P, \quad (5)$$

$$E_X(T,P) = 1.981 - [4.60 \times 10^{-4} T^2 / (T + 204)] - 0.0008P, \quad (6)$$

$$E_{\Gamma}(T,P) = 3.130 - [5.0 \times 10^{-4} T^2 / (T + 204)] + 0.0102P, \quad (7)$$

$$E_X(T,P) = 2.229 - [4.60 \times 10^{-4} T^2 / (T + 204)] - 0.0008P. \quad (8)$$

Equations (5) and (6) and (7) and (8) are applied to gap energies (in eV) in GaAs and AlAs, respectively, while the entropy factor is introduced in the energy of the  $\Gamma$  shallow states ( $S_{sd} = 0.54$  meV/K) and deep states ( $S_{DX} = 0.35$  meV/K).<sup>17</sup> Thus the energy was expressed as

$$E = H - TS, \quad (9)$$

where  $H$  and  $S$  denote the enthalpy and the entropy of the level, respectively. The fit of the carrier concentration at various pressures needs to account for the existence of two  $DX$  donors ( $DX_0$  and  $DX_1$ , respectively, in samples HB11  $\delta$ -doped in GaAs,  $DX_3$  and  $DX_2$ , respectively, in samples HC01  $\delta$ -doped in AlAs). Note that a previously developed interdiffusion model<sup>17</sup> applied on sample HC01 gives an outdiffusion of the silicon atoms from AlAs around 40%. A shallow donor linked with the  $\Gamma$  miniband (5 meV) is taken into account in all the

TABLE II. Difference in the energies of the deep silicon donors. The reference of the energy is taken to be the energy of the  $DX_0$  state.

| Energy (meV) | Ref. 12 | Ref. 14 | Ref. 24 | Ref. 25 | Ref. 26 | This work |
|--------------|---------|---------|---------|---------|---------|-----------|
| $DX_0$       | 0       | 0       | 0       | 0       | 0       | 0         |
| $DX_1$       | -28     | -50     | -20     | -50     | -46     | -40       |
| $DX_2$       | -47     | -70     | -25     | -70     | -92     | -80       |
| $DX_3$       | -58     | -120    | -38     | -100    | -138    | -130      |

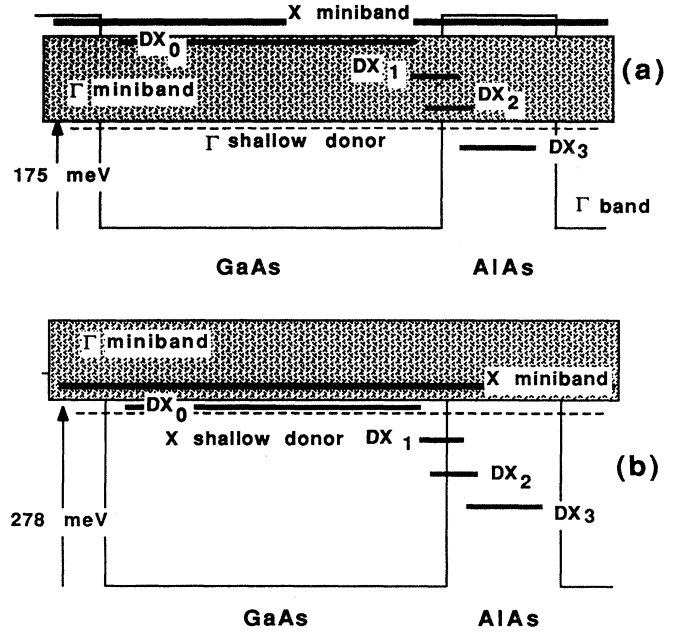


FIG. 11. Energetical diagram of the superlattice at two pressures:  $P = 0$  kbar (a) and  $P = 9$  kbar (b). Shallow donors linked to the miniband and spatially separated  $DX$  deep donors are reported.

samples. The  $DX$  relative energies are derived numerically and collected in Table II with those given recently in the literature for the silicon donor in  $Al_xGa_{1-x}As:Si$ .<sup>12,24-26</sup> Figure 11 shows the energetical diagram of the  $DX$  center in our superlattices at two pressures. The reference in energy is the  $\Gamma$ -band energy in GaAs wells. We found the values 270, 230, 190, and 140 meV for the  $DX_i$  ground-state enthalpies ( $i = 0, 1, 2,$  and  $3$ , respectively). The spectroscopy of the  $DX$  levels is made by increasing pressure in order to move the  $\Gamma$  miniband up to the  $\Gamma$ - $X$  crossover. Figure 12 shows the dependence of the miniband minima, associated shallow levels, and  $DX$  energies, respectively, as calculated as a function of pressure using Eqs. (5)–(8).

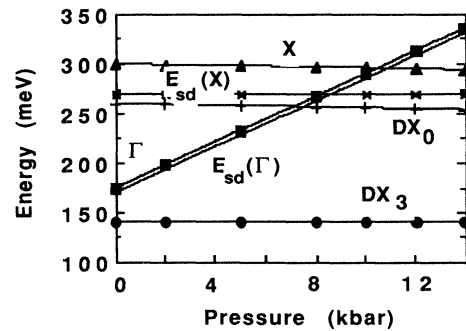


FIG. 12. Energy of  $\Gamma$  and  $X$  minibands and associated shallow-donor levels as a function of hydrostatic pressure at room temperature. The reference in energy is the  $\Gamma$  band in GaAs. Only the energies of the two extreme levels  $DX_0$  and  $DX_3$  are reported.

## V. DISCUSSION AND CONCLUSION

When considering values in Table II, we find that, depending on the experiment [Hall effect and capture/emission kinetics in three-dimensional (3D) layers or 2D heterostructures] and method of energy extraction, the spreading of the ionization energies is large. Note that values are extrapolated at  $x=0$  for alloys with  $0.15 < x < 0.33$  such that the contribution of  $DX_3$  is small. In contrast, the spatial separation of Al and Ga atoms in superlattices leads to a more accurate energy determination between  $DX_0$  and  $DX_3$  states. The best fit of electron-capture kinetics is obtained in the alloy taking into account the full  $35 \times 4$  statistics and the spatial correlation of charges.<sup>24</sup> Indeed, Eq. (3) indicates that because of the bistable character of the  $DX$  center (shallow or deep donor), a gain in energy is obtained due to the coexistence of the ionized donor  $d^+$  and negatively charged state  $DX^-$  (like dipoles  $d^+DX^-$ ). Our model did not account for charge correlation effects but the energetical positive shift did not exceed 10–20 meV.<sup>17,24</sup> Consequently our results confirm the energy splitting of the  $DX$  center from AlAs to GaAs by an amount of 130 meV.

Note that in a preceding paper<sup>17</sup> we found the energy splitting to be larger than 60 meV. This value was underestimated because the samples were not planar doped such that the silicon segregation in the adjacent layers

was large. Consequently, the  $DX$  levels were mixed, and the interpretation in terms of only two levels ( $DX_0$  and  $DX_3$ ) was inaccurate since the existence of additional levels ( $DX_1$  and  $DX_2$ ) and the high energy of the  $\Gamma$  miniband (245 meV instead of 175 meV in the present study) led to an equivalent  $DX_0$  state with an underestimated energy and an equivalent  $DX_3$  state with an overestimated energy in those samples. It is worth noticing that Baba *et al.*<sup>14</sup> used superlattices with a low Al content (only 1 ML of AlAs embedded in 14 ML of GaAs) such that the  $DX_3$  energy (175 meV) could be also overestimated.

In conclusion, we used hydrostatic pressure to derive the ionization energy of the silicon donor in GaAs, AlAs, and in an Al/Ga alloying environment. Hall measurements carried out under pressure or after nonequilibrium situations (electron capture in the PPC regime or electron emission after PIFO) showed up to four  $DX$  levels. Only the  $DX_3$  state was in the gap of the superlattice at ambient pressure. Thus by applying pressure, the miniband edge crosses over the high-lying levels, and a spectroscopy of the  $DX_i$  levels is performed, the ionization energies being extracted from the Hall data.

Note that this pressure-induced spectroscopy can be performed only in short-period superlattices with low outdiffusion of dopants (i.e., in planar-doped superlattices), having an Al content which allows us to explore a wide range of energies (i.e., far from the  $\Gamma$ - $X$  crossover).

\* Author to whom all correspondence should be sent.

<sup>1</sup>D. V. Lang, in *Deep Centers in Semiconductors*, edited by S.T. Pantelides (Gordon and Breach, New York, 1986), p. 489, and references therein (1986).

<sup>2</sup>P. M. Mooney, *J. Appl. Phys.* **67**, R1 (1990), and references therein.

<sup>3</sup>D. J. Chadi and K. J. Chang, *Phys. Rev. B* **39**, 10063 (1989).

<sup>4</sup>T. N. Theis, P. M. Mooney, and S. L. Wright, *Phys. Rev. Lett.* **60**, 361 (1988).

<sup>5</sup>V. Mosser, S. Contreras, J. L. Robert, R. Piotrkowski, W. Zawadzki, and J. F. Rochette, *Phys. Rev. Lett.* **66**, 1737 (1991).

<sup>6</sup>L. Dobaczewski and P. Kaczor, *Phys. Rev. B* **44**, 8621 (1991).

<sup>7</sup>G. Brunthaler and K. Köhler, *Appl. Phys. Lett.* **57**, 2225 (1990).

<sup>8</sup>*The DX Center and Other Metastable Defects in Semiconductors* [Semicond. Sci. Technol. **6** (1991)].

<sup>9</sup>N. Lifshitz, A. Jayaraman, R. A. Logan, and H. C. Card, *Phys. Rev. B* **21**, 670 (1980).

<sup>10</sup>E. Calleja, F. Garcia, A. Gomez, E. Munoz, P. M. Mooney, T. N. Morgan, and S. L. Wright, *Appl. Phys. Lett.* **56**, 934 (1990).

<sup>11</sup>R. Piotrkowski, E. Litwin-Staszewska, P. Lorenzini, and J. L. Robert, *Semicond. Sci. Technol.* **7**, 103 (1992).

<sup>12</sup>Z. Wilamowski, J. Kossut, W. Jantsch, and G. Ostermayer, *Semicond. Sci. Technol.* **6**, B38 (1991).

<sup>13</sup>S. Ababou, J. J. Marchand, L. Mayet, G. Guillot, and F. Mollot, *Superlatt. Microstruct.* **7**, 283 (1990).

<sup>14</sup>T. Baba, M. Mizuta, T. Fujisawa, J. Oshino, and H. Kukimoto, *Jpn. J. Appl. Phys.* **28**, L891 (1989).

<sup>15</sup>J. Sicart, P. Jeanjean, J. L. Robert, W. Zawadzki, F. Mollot, and R. Planel, *Phys. Rev. B* **43**, 7351 (1991).

<sup>16</sup>G. Bastard, *Wave Mechanics Applied to Semiconductor Heterostructures* (Editions de Physique, Les Ulis, 1988).

<sup>17</sup>P. Sellitto, P. Jeanjean, J. Sicart, J. L. Robert, and R. Planel, *J. Appl. Phys.* **74**, 7166 (1993).

<sup>18</sup>R. J. Nelson, *Appl. Phys. Lett.* **31**, 351 (1977).

<sup>19</sup>T. Suski, *Mater. Sci. Forum* **143-147**, 975 (1994).

<sup>20</sup>L. Hart, P. F. Fewster, M. J. Ashwin, M. R. Fahy, and R. C. Newman, *Mater. Sci. Forum* **143-147**, 647 (1994).

<sup>21</sup>D. C. Look, *Phys. Rev. B* **24**, 5852 (1981).

<sup>22</sup>T. N. Theis, P. M. Mooney, and B. D. Parker, *J. Electron. Mater.* **20**, 35 (1991).

<sup>23</sup>S. Adachi, *J. Appl. Phys.* **58**, R1 (1985); D. E. Apnes, *Phys. Rev. B* **14**, 5331 (1976).

<sup>24</sup>G. Stöger, G. Brunthaler, G. Ostermayer, W. Jantsch, Z. Wilamowski, and K. Köhler, *Mater. Sci. Forum* **143-147**, 1149 (1994). These authors take into account all possible combinations of energy levels due to the Al environment of the silicon atom (35 types of  $DX$  centers with four levels each) instead of the simple statistics (four times one). The probability to find a certain type depends on the Al content of the  $Al_xGa_{1-x}As$  alloy. Moreover, the  $35 \times 4$  statistics includes the possibility of a redistribution of electrons among the states in each  $DX$  center.

<sup>25</sup>G. Brunthaler, M. Seto, G. Stöger, G. Ostermayer, and K. Köhler, *Mater. Sci. Forum Vols.* **143-147**, 641 (1994).

<sup>26</sup>V. Mosser, S. Contreras, P. Lorenzini, and J. L. Robert, *Mater. Sci. Forum* **143-147**, 1117 (1994).